Facile Synthesis of Lignosulfonate-graphene Porous Hydrogel for Effective Removal of Cr(VI) from Aqueous Solution

Zhili Zhang,[a] Fengfeng Li,[b] Xingxiang Ji,[b,*] Jiachuan Chen,[b,*] Guihua Yang,[b] and Lucian A. Lucia [b,c]

A green and facile fabrication strategy for synthesis of lignosulfonate-graphene porous hydrogel (LGPH) was designed *via* incorporation of lignosulfonate (LS) into graphene oxide (GO). This process was achieved by a simple self-assembly method at low temperature, with LS serving as surface functionalization agent. Benefiting from the abundant functional groups of LS and the large surface areas of graphene oxide, the prepared LGPH hydrogel displayed 3D interconnected pores and exhibited an excellent adsorption capacity for Cr(VI) (601.2 mg/g) ions dissolved in water. Importantly, the free-standing LGPH was easily separated from water after the adsorption process, and the adsorption capacities of Cr(VI) onto LGPH maintained 439.1 mg/g after 5 adsorption-desorption cycles. The cost-effectiveness and environmental friendliness of LGPH make it a promising material for removing heavy metals from wastewater.

Keywords: Lignosulfonate; Graphene oxide; Adsorption; Heavy metals

*Contact information: a: School of Light Industry and Engineering, Qilu University of Technology, Jinan 250353, PR China; b: Key Laboratory of Pulp and Paper Science and Technology of Ministry of Education, Qilu University of Technology, Jinan, 250353, PR China; c: The Laboratory of Soft Materials and Green Chemistry, Department of Forest Biomaterials, North Carolina State University, Raleigh, NC, 27695, U.S.A; *Corresponding authors: xxjt78@163.com; chenjc@spu.edu.cn*

INTRODUCTION

Water pollution by Cr(VI) is a major global problem because of its detrimental and toxicological impacts on the environment and humans (Gao *et al.* 2018; Sun *et al.* 2019). Considering the toxicological impacts on animals and humans, water treatment is needed, and various techniques such as membrane filtration (Chitpong and Husson 2017), chemical coagulation (Yao *et al.* 2017), electrochemical oxidation, bioremediation, microwave catalysis (Wang *et al.* 2019), photocatalytic purification (Huang *et al.* 2017), and adsorption (Liang *et al.* 2019) have been devoted for wastewater treatment. Adsorption is superior to other techniques to remove heavy metal ions due to its lower operating cost, convenience of design, and effective elimination of the secondary contamination (Zhang and Zhang 2014; Wang *et al.* 2018; Yang *et al.* 2018a). A variety of adsorbents have been studied for Cr(VI) removal, including activated carbons, carbon nanotubes, functionalized magnetic nanoparticles, biomass, and synthetic polymers (Chang *et al.* 2017; Xu *et al.* 2017). Though the above mentioned adsorbents have been used for the removal of Cr(VI), most of these conventional adsorbents have limitations such as high cost of preparation or difficult recovery from wastewater. To overcome these limitations, an economical and eco-friendly adsorbent with excellent adsorbing performance is needed.

Recently, self-assembled graphene materials including hydrogels and aerogels have been investigated as adsorbents. Hydrogels with three-dimensional network structures have attracted intense interest in wastewater treatment, due to its unique physical and chemical properties (Wang *et al.* 2017). Graphene oxide (GO) shows good affinity with many soluble cationic or aromatic pollutants *via* electrostatic or π-conjugate interactions (Yu *et al.* 2013; Vu *et al.* 2017). Nevertheless, the absorption capacity is greatly reduced due to the reduction in the number of reactive groups during the self-assembly process (Xu *et al.* 2010). Thus, an effective method to enhance the absorption capacity is to increase the content of reactive groups of these materials. Biomass chemical components, such as cellulose, lignosulfonate, and chitosan, are often incorporated into adsorbents to enhance their performance (Akram *et al.* 2017). Lignosulfonate is the most popular compound due to its biodegradability, renewability, and good metal ion adsorption capacities (Myglovets *et al.* 2014). For example, Yang *et al.* (2014) prepared a lignosulfonate-graphene oxide-polyaniline (LS-GO-PANI) by *in situ* polymerization using lignosulfonate and graphene oxide. Li *et al.* (2016) reported a lignosulfonate-modified graphene hydrogel (LS-GH) fabricated from lignosulfonate and graphene oxide sheets *via* hydrothermal method. These reports suggested that the lignosulfonate incorporation improved the adsorption ability of heavy metal ions. For LS-GO-PANI, the electrostatic interactions between sulfonic anions on the LS chain and polyaniline units results in the active functional groups in LS that is consumed and generated large amounts of organic waste. Additionally, the tight composite structure greatly limits the availability of active surface area and thus limits adsorption. The hydrothermal method requires high temperature (180 °C), which can be regarded as unfavorable for commercial applications due to its high energy consumption.

To overcome the challenges mentioned above, a hydrogel functionalized with LS, a byproduct of the pulp and paper industry, was developed for the removal of Cr(VI) ions from aqueous solution. In this study, freestanding LGPH was prepared *via* an eco-friendly one-step method at low temperature. The abundant functional groups of LGPH were expected to be the active sites for heavy metals through electrostatic attraction. The effects of initial pH, adsorbent concentration, and contact time on the adsorption of Cr(VI) ions from aqueous solutions were also studied by batch experiments. The kinetic and equilibrium parameters were calculated to investigate the adsorption performance of LGPH. The LGPH exhibited ultrahigh adsorption ability for Cr(VI), which could have great potential application in removing heavy metals ions from industrial wastewater.

EXPERIMENTAL

Materials

Lignosulfonate (LS, $C_{20}H_{24}Na_2O_{10}S_2$, MW 534.51), natural graphite powder (325 mesh, purity of 99.95%), vitamin C (VC, purity of 99.5%), $K_2Cr_2O_7$, and other reagents were of analytical grade and obtained from Aladdin Industrial Corporation (Shanghai, China). All chemicals were used as received without further purification. The experimental Cr(VI) solution was prepared by dissolving $K_2Cr_2O_7$ in deionized water.

Methods

Synthesis of graphene oxide

Graphene oxide (GO) was synthesized from natural graphite powder using a modified Hummers's method (Hummers and Offeman 2002). To avoid aggregation of GO

during the drying process, the GO sample was obtained by freeze-drying. The dried GO sample was dispersed in water by ultrasonication for 30 min to make an aqueous dispersion at a concentration of 2.0 mg/mL.

Synthesis of GPH and LGPH

The adsorbent LGPH was prepared as follows. First, LS (10 mg), VC (100 mg), and GO aqueous dispersion (10 mL) were added to a 25 mL glass flask. The reaction mixture was stirred at room temperature until it became a stable suspension. The mixture was then transferred to a 15 mL sealed glass bottle and autoclaved at 60 °C for 2 h. The autoclave was allowed to cool to room temperature, and the LGPH was removed. A control sample of GPH was prepared using the same procedure without LS addition.

Material characterization

The FT-IR spectra were obtained on a Vertex 70 instrument (Bruker, Rheinstetten, Germany) in the range of 500 cm^{-1} to 4000 cm^{-1} at a resolution of 0.5 cm^{-1}. An atomic force microscope (AFM, Nanoscope III Veeco Co. Ltd., Santa Barbara, USA) was employed to characterize the GO samples. Samples for AFM analysis were prepared on freshly cleaved mica. X-ray diffraction (XRD) patterns of dried samples were measured with a Bruker D8 Advance diffractometer. The conditions of test were: the tube current and voltage at 20 mA and 30 kV, respectively, Cu target (λ = 0.15418 nm), and data were collected from the 2θ angular regions between 5° and 60°. The thermal stability of the dried samples was investigated using a TGA Q500 (TA Instruments, New Castle DE, USA). The samples were heated in an aluminum crucible to 650 °C at a heating rate of 20 °C/min. The surface morphology of dried samples was analyzed by scanning electron microscopy (SEM; Bruker) at 10 kV. The samples for SEM analysis were coated with a thin layer of gold (2 nm) by sputtering to promote conductivity before SEM observation. The instrument ASAP 2460 was employed to observe the nitrogen adsorption isotherms at -196 °C. The specific surface area was evaluated from the adsorption branch of the isotherm using Brunauer-Emmett-Teller theory (BET). X-ray photoelectron spectroscopy (XPS) was conducted on a Axis Ultra DLD spectrometer (Kratos, Manchester, UK) with monochrome Al Kα radiation (hv = 1486.6 eV).

Adsorption experiments

Approximately 100 mL of Cr(VI) solution and the composite (8 mg) were loaded in a 200 mL conical flask and placed it in an air table with 200 rpm stirring speed at 25 °C for 12 h to reach equilibrium. The desired pH value was adjusted using 0.1 M HCl or 0.1 M NaOH solution. After a desired adsorption period (0 to 600 min), the composite was removed gently with forceps from the solution, and the concentration of Cr(VI) after adsorption was measured by atomic absorption spectrophotometer (Z-2000, Hitachi Ltd., Tokyo, Japan).

The adsorbed amount of Cr(VI) on the adsorbent was calculated according to the following Eq. 1,

$$Q = \frac{(C_0 - C_e) \times V}{m} \quad (1)$$

where Q is the adsorption capacity (mg/g); C_0 and C_e are the Cr(VI) concentration before and after adsorption (mg/L), respectively; V is the initial volume of the Cr(VI) solution (L); m is the weight of the composite (g).

RESULTS AND DISCUSSION

Characterization of Samples

After heating the LS, VC, and GO aqueous dispersions at 60 °C for 2 h, a black cylinder-like LS-functionalized graphene hydrogel appeared at the bottom of the glass vessel, without any suspended GO sheets or LS in the solution (Fig. 1a). Figures 1b and 1c show, respectively, a representative AFM image of a GO nanosheet and its height profile. The cross-sectional analysis showed that the thickness of the GO sheets were in the ranges of 0.98 nm, which illustrated that the GO sheet was about one-atom-thick graphene oxide (Chang *et al.* 2010). The LGPH were prepared through a facile one-step hydrothermal method. The results indicated a well-defined and interconnected 3D porous network as revealed by SEM images of freeze-dried samples (Figs. 1d to 1e). The π-π stacking of graphene sheets plays an important role in the formation 3D network porous structure of GPH. For LGPH, besides the above factor, the π-π conjugation and hydrogen bonding between graphene sheets and LS contributed to the successful construction of 3D porous structure, favoring the transport and adsorption of metal ions (Zhou *et al.* 2016). Furthermore, the multilevel pore structure of LGPH provided large specific surface area (473.5 m^2/g) that was higher than that of GPH (261.7 m^2/g). These findings were confirmed by the nitrogen adsorption-desorption isotherms in Fig. 2a.

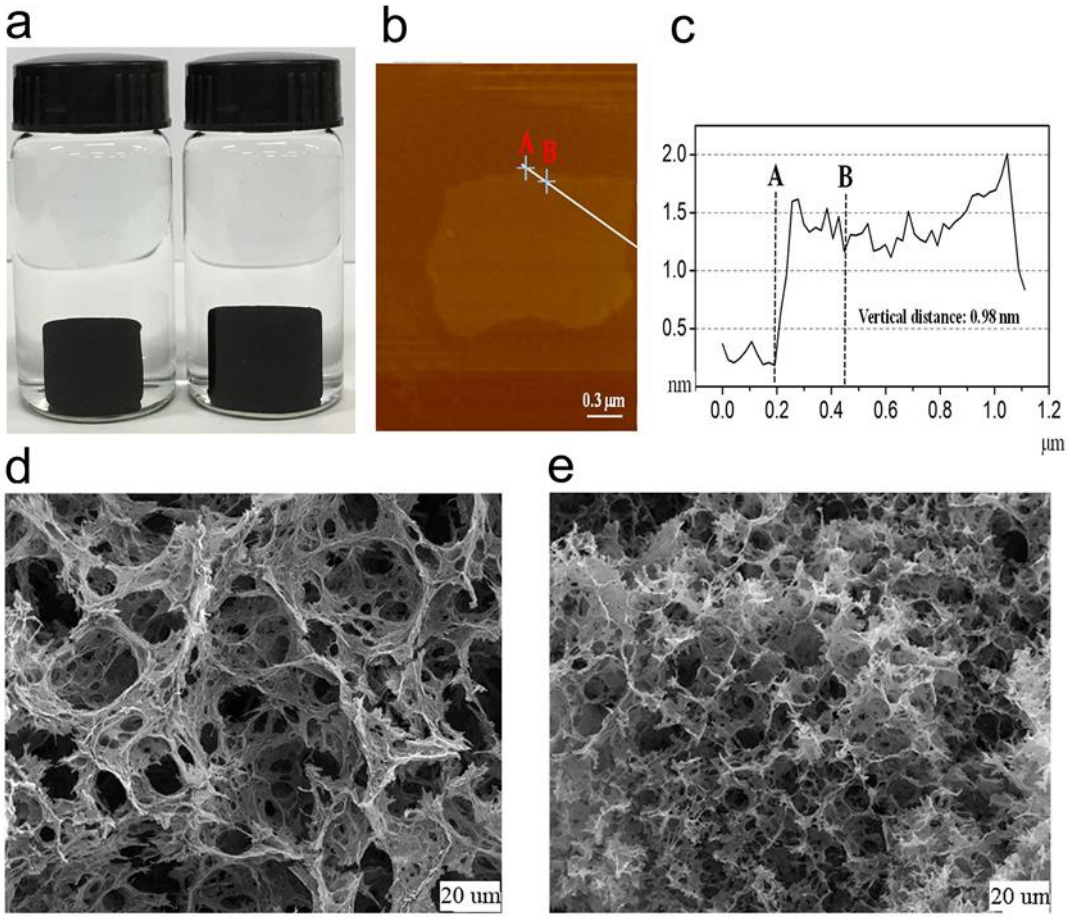

Fig. 1. (a) Photographs of monolithic materials of GPH (left) and LGPH (right); (b) AFM image of GO sheet; (c) GO sheet height profile; SEM micrograph of GPH (d) and LGPH (e)

The large surface area of LGPH also contributes to the high adsorption capacity. (Zhang *et al*. 2019a,b). During the hydrothermal reaction, LS penetrated into graphene sheets through non-covalent interactions, such as π-π conjugation and hydrogen bonding. The negatively charged LS molecules spread in the interlayer of graphene sheets, which prevents the restacking of graphene sheets through electrostatic repulsion. Consequently, the specific surface area of LGPH was increased compared with that of GPH, improving the adsorption capacity to metal ions (Yi and Zhang 2008).

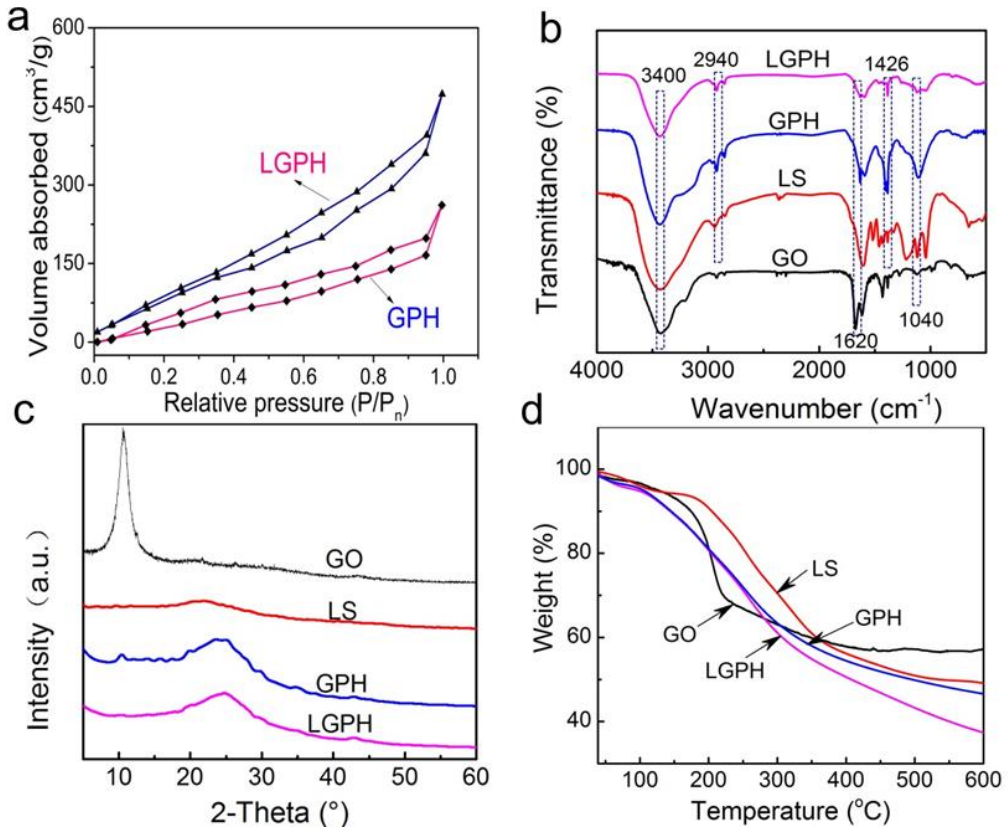

Fig. 2. (a) BET plots of GPH and LGPH; (b) FT-IR spectra; (c) XRD spectra; (d)TGA curves of GO, LS, GPH, and LGPH

As shown in Fig. 2b, the characteristic peaks at 3400 cm^{-1}, 1720 cm^{-1}, 1620 cm^{-1}, 1200 cm^{-1}, and 1061 cm^{-1} can be attributed to O-H, C=O, C-C, C-O-C, and C-O groups of GO sheets, respectively (Zhao *et al.* 2015). These hydrophilic groups on the surface are very important to improve the interaction between LS and GO sheets. As shown in the FT-IR spectra of LS, the peak at 3408 cm^{-1} was due to the O–H stretching. The bands around 1219 cm^{-1} and 1040 cm^{-1} are attributed to sulfonic acid groups (He *et al.* 2013). The band at 618 cm^{-1} was due to the C-S stretching vibration. The characteristic peaks at 3400 cm^{-1} and 1620 cm^{-1} belonging to GO can also be observed in the spectra of GPH and LGPH. This indicated that there exist a certain number of functional groups on reduced GO sheets. Additionally, compared with the GPH, the S=O symmetric stretching at 1040 cm^{-1} belonging to LS was also observed, which indicated the proposed formation of LGPH. The existences of sulfonic acid groups was evident from the FTIR spectra and these groups were responsible for improving its adsorption capacity to water and metal ions. The change at ~3400 cm^{-1} could be ascribed to the strong interaction through hydrogen bonds and π-π conjugation between LS and GO sheets.

The XRD patterns of GO, LS, GPH, and LGPH are presented in Fig. 2c. The GO pattern showed a peak at ~10.7° corresponding to the (001) inter-planar spacing of 8.30 Å caused by the oxygen-rich groups on both sides of the sheets and the water molecules trapped between the sheets (Marcano *et al.* 2010). The interlayer spacing of the freeze-dried GPH and LGPH was calculated to be 3.69 Å, and 3.65 Å, respectively. This value was much lower than that of GO (8.30 Å), which suggested the presence of π-π stacking between graphene sheets in the composites and also the presence of a certain number of functional groups on reduced GO sheets (Murugan *et al.* 2009). For GPH, the reduced GO sheets can encapsulate water in the process of self-assembly due to the presence of residual hydrophilic oxygenated groups. For LGPH, in addition to functional groups on reduced GO sheets, the hydrophilic groups of LS could also capture a multitude of water. Because of this factor and the stacking of graphene sheets, the composites can be successfully synthesized by one-step method. For LS, the broad peak between 20° and 30° was attributed to its low graphitization and amorphous nature. Furthermore, there has been no distinction between the XRD patterns of GPH and LGPH, which indicated that LS was uniformly distributed on GO.

The TG analyses were employed to study the thermal decomposition of composites. The TG curve of GO, LS, GPH, and LGPH are shown in Fig. 2d. For GO, the range of maximum decomposition temperature (T_{max}) was between 160 °C and 250 °C. Thermal degradation in this range was due to the decomposition of oxygen-containing groups on the surface of reduced GO sheets (Mianehrow *et al.* 2015). For LS, the range of T_{max} was about 180 °C to 300 °C, which was attributed to the fragmentation of inter-unit linkages. The T_{max} of LGPH was 266.9 °C, while the T_{max} of GPH was 260.0 °C. The incorporation of LS into the LGPH slightly improved the thermal stability as evaluated from T_{max}. The T_{max} of LGPH was higher than that of GPH. Therefore, the addition of LS was attributed to enhance the thermal stability. One possible reason for this improvement is due to the π-π conjugation and hydrogen bonding between graphene sheets and LS (Yao *et al.* 2003).

The XPS patterns were used to illustrate the elemental compositions of GPH and LGPH composites. As shown in Figs. 3a and 3b, the C1s in the XPS spectra of GPH and LGPH clearly revealed the existence of four types of carbons with various chemical valences: C-C/C=C (284.6 eV), C-O (286.1 eV), C=O (287.7 eV), and C-O=O (289.1 eV) (Yang *et al.* 2018b).

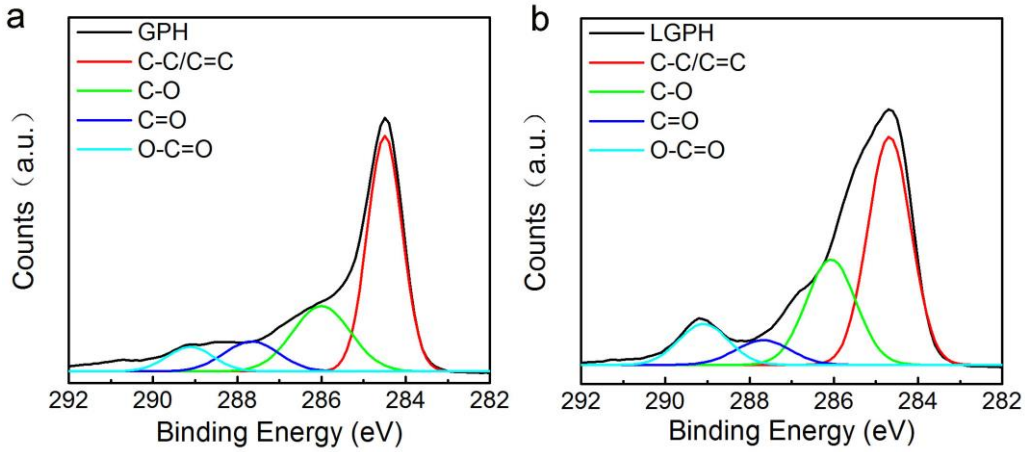

Fig. 3. (a)XPS patterns of GPH; (b) XPS patterns of LGPH

Compared to GPH, the intensity of C-O peak (286.1 eV) was increased, which indicated that LS incorporation was beneficial for improving the atomic contents of oxygen in LGPH and ultimately enhanced the adsorption ability for Cr(VI) ion

Formation Mechanism of LGPH

According to the above-mentioned analysis, a possible mechanism was proposed to explain the formation of LGPH. As illustrated in Fig. 4, the surface of GO sheets contains many oxygen-containing hydrophilic functional groups, which makes GO easily dispersed in water (Zhang and Yang 2017). Similarly, LS molecule also contains large number functional groups such as hydroxyl and sulfonic groups (Gupta *et al.* 2013). At first, GO and LS were homogeneously dispersed in the solution. As the reaction proceeded, the flexible graphene sheets were random stacked to form a 3D network structure. Further, this self-assembly process was driven by strong interactions between graphene sheets, such as π-π stacking, hydrogen bonding, and inclusion interaction. At the end of the reaction, there were a certain number of functional groups on reduced GO sheets (as demonstrated by FT-IR analysis). During the self-assembly process, the LS molecule was attached on the surface of reduced GO sheets *via* hydrogen bonding between the OH groups of LS and the OH and COOH groups of reduced GO sheets. Thus the incorporation of LS effectively improved the content of adsorption sites of LGPH (Yang *et al.* 2010).

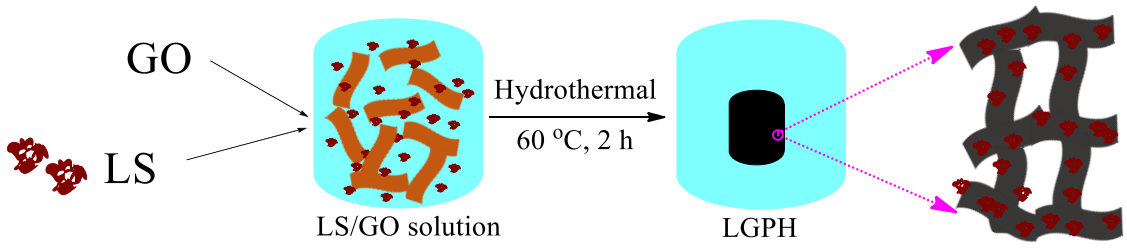

Fig. 4. Schematic diagram of the green synthesis of LCH

Adsorption of Cr(VI)

The adsorption performance was noticeably affected by initial pH values of the adsorption medium because of the surface charge distribution and availability of binding sites of the adsorbents, and chromium species (Karnitz *et al.* 2007). Changes in the pH can affect the surface charges of the adsorbents by changing the ionization state of functional groups. In this study, the adsorption experiment was carried out at a Cr(VI) concentration of 400 mg/L, and a temperature of 25 °C for 12 h. The initial pH values of the solution were adjusted to 2.0, 3.0, 4.0, 5.0, 6.0, and 7.0. Figure 5a shows the zeta potential of LGPH, which clearly indicated that the surface charges of composites were pH-dependent. The isoelectric point of the LGPH was found to be at pH 2.5, and its surface charge was negative above the isoelectric point. The negative shift in surface charge of LGPH in the range of pH 3 to 7 suggested that the adsorbents were more protonated, which was expected to provide more binding sites and in favor of the adsorption of Cr(VI) *via* electrostatic attraction. At higher pH, the LGPH may carry more negative charges, which could increase the electrostatic interactions between surface active sites and Cr(VI) ions. However, the adsorption capacity was affected by many other forces, especially the chromium species in the solution. At low pH, portion of the Cr(VI) may be reduced to Cr(III) and stay octahedral hexaaquo ion $Cr(H_2O)_6^{3+}$ in solution, which would inhibit the adsorption by the protonated sulfonic groups (Gallios and Vaclavikova 2007). As shown in the Fig. 5b, the adsorption

capacity of Cr(VI) on the LGPH increase with increasing the initial pH value from 2 to 3. The adsorption capacity of Cr(VI) was low, ~494 mg/g at pH 2, but increased to 600 mg/g at pH 3. Thus, the chromium adsorption by LGPH was pH-dependent, and lower pH might be more beneficial to the uptake of Cr(VI). Therefore, later studies were carried out at a fixed pH value of 3.0.

The effects of contact time on the adsorption capacities of LGPH were also investigated, as reported in Fig. 5c. The adsorption experiment was carried out at a Cr(VI) concentration of 400 mg/L, a temperature of 25 °C, and a fixed pH value of 3.0. When the contact time was increased, the adsorption capacity of Cr(VI) increased substantially. When the adsorption time was 60 min, 400 mg/g adsorption was achieved. Moreover, the equilibrium balance of adsorption was reached at 480 min, in which a higher adsorption capacity (601.2 mg/g) was obtained. The fast adsorption of Cr(VI) was attributed to the porous structure and the large amounts of functional groups on LGPH (Li *et al.* 2015).

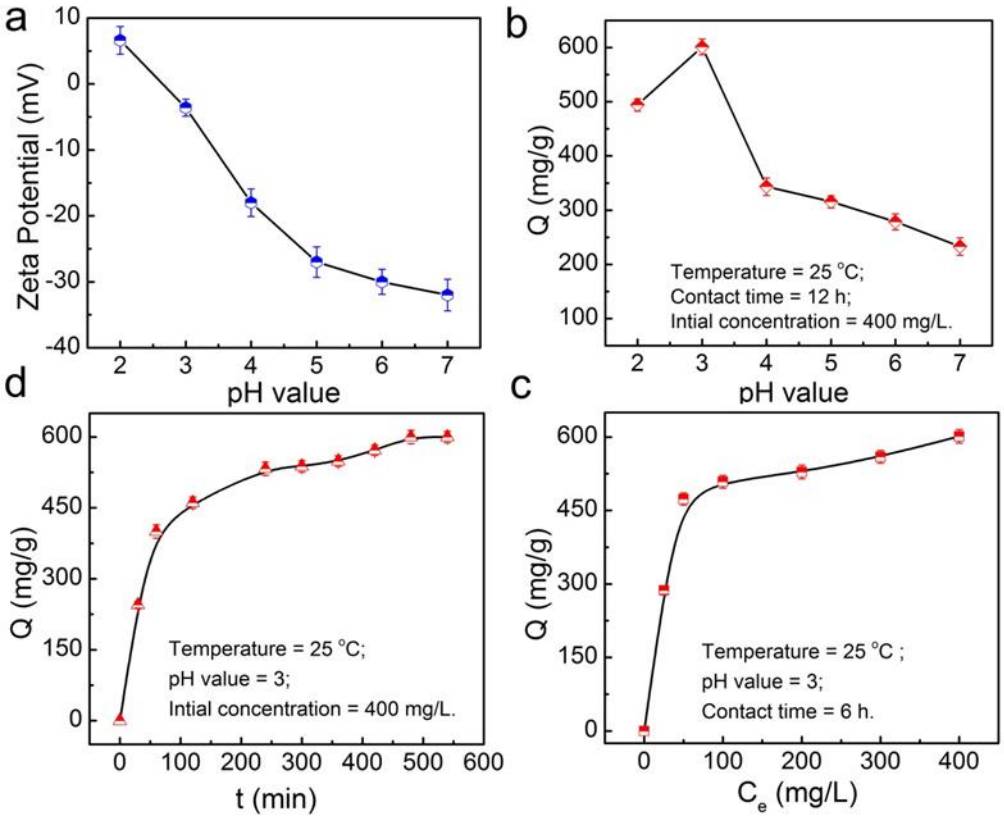

Fig. 5. (a) Zeta potentials of LGPH; (b) Effect of the initial pH value on adsorption capacities; (c) Effect of the contact time on adsorption capacities; (d) Effect of initial Cr(VI) ions concentration on adsorption capacities

The effects of initial Cr(VI) ions concentration on adsorption capacities of Cr(VI) onto LGPH were also studied at pH 3.0 for a contact time of 480 min and at the LGPH concentrations ranging from zero to 400 mg/L. As can be seen from the Fig. 5d, when the initial concentration was increased from 25 mg/L to 100 mg/L, the adsorption capacities of Cr(VI) increased up to 508.5 mg/g from 317.1 mg/g. Furthermore, when the initial Cr(VI) concentration is 400 mg/L, the adsorption capacity of LGPH was 601.2 mg/g. However, the adsorption capacity of GPH was only 434.2 mg/g under the same condition. Evidently, the adsorption capacity of LGPH was significantly improved. The changes in removal

efficiency may be ascribed to the following reason. It is well known that large specific surface area and more active sites are very important to improve adsorption capacity.

The observed high performance of LGPH is very valuable to reduce the wastewater treatment cost and realize commercialization. The metal ion adsorption onto LGPH is a reversible process and it is possible to regenerate the adsorbent for reuse. Desorption of metal ions from LGPH surface depends on pH; hence desorption of metal ions is also possible by controlling the pH of the regeneration solution. Many studies have identified acid solution (HNO_3, HCl, H_2SO_4) is a most effective eluent for the desorption process. Li *et al.* (2005) found that the desorption of the metal ions increased with decreasing pH of the regeneration eluent. Liang *et al.* (2004) reported in their work that the Mn^{2+} ions could be effectively desorbed from the adsorbent using a 1.0 M HNO_3 solution. Yildiz *et al.* (2017) reported that 0.1 M HCI and 0.1 M H_2SO_4 had high elution efficiencies and ~90% Cu^{2+} desorption was achieved. In this paper, desorption experiments were carried out by employing 0.1 M HCl solution. The results showed that as the adsorption–desorption cycles increased, the adsorption capacities decreased slightly. The adsorption capacities of Cr(VI) onto LGPH maintained 439.1 mg/g even after 5 cycles, which indicated that LGPH has excellent reusability and has potential application for commercial use. Furthermore, the good mechanical properties of LGPH were maintained after adsorption.

Mathematical Models

Both pseudo-first-order and pseudo-second-order models were employed to fit the experimentally obtained adsorption data (Park *et al.* 2019). The pseudo-first-order and pseudo-second-order equations were expressed by Eqs. 2 and 3,

$$\ln(Q_e - Q_t) = \ln Q_e - k_1 t \quad (2)$$

$$\frac{t}{Q_t} = \frac{1}{k_2 Q_e^2} + \frac{t}{Q_e} \quad (3)$$

where k_1 and k_2 represent the pseudo-first-order and pseudo-second-order rate constants. Q_t is the amount of Cr(VI) adsorbed per adsorbent (mg/g) at time t. The parameters of the pseudo-first-order and pseudo-second-order equations for the adsorption of Cr(VI) onto LGPH are listed in Fig. 6a and Table 1. Compared with the pseudo-first-order kinetic model, the pseudo-second-order kinetic model exhibited much higher coefficient of determination (R^2). In addition, the numerical results calculated from pseudo-second-order equation are close to the measured data, which indicated that the pseudo-second-order model was a more applicable model to the kinetics of Cr(VI) adsorption.

In addition, both Langmuir and Freundlich isotherm models were used to describe and analyze the adsorption equilibriums, as described by Eqs. 4 and 5,

$$\frac{C_e}{Q_e} = \frac{C_e}{Q_m} + \frac{1}{K_L Q_m} \quad (4)$$

$$lnQ_e = \frac{1}{n}\ln C_e + lnK_F \quad (5)$$

where Q_e is the amount of Cr(VI) adsorbed (mg/g) at equilibrium, Qm (mg/g) and K_L are the Langmuir constants related to the saturated adsorption capacity and adsorption energy, respectively. The Freundlich constants K_F and n were related to the sorption capacity and

sorption intensity, respectively. The fit line and corresponding parameters for the sample obtained from the lines are displayed in Fig. 6b and Table 1.

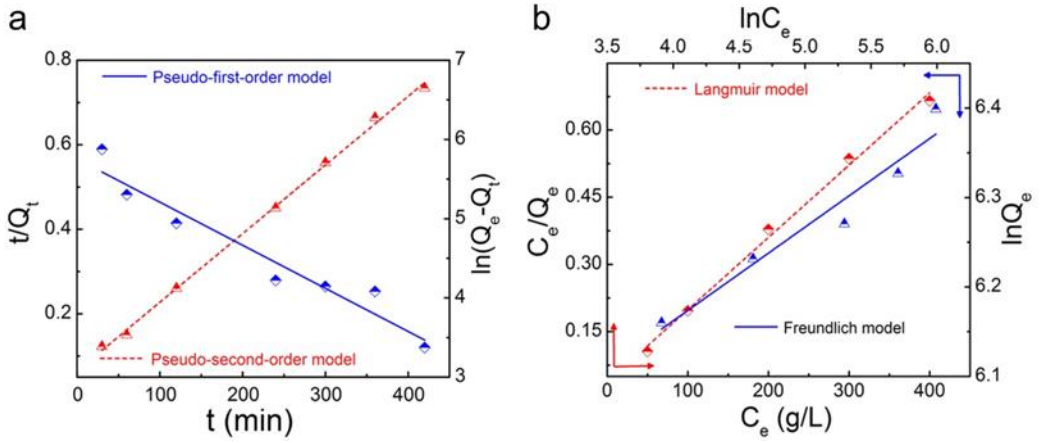

Fig. 6. (a) Fitting results for the Pseudo-first-order and pseudo-second-order kinetic models (C_0 = 400 mg/L, T = 25 °C, pH = 3.0); (b) Fitting results for the Langmuir and Freundlich isotherm models (T = 25 °C, pH = 3.0, t = 6 h)

Table 1. Kinetic Parameters and Adsorption Isotherm Parameters for the Adsorption of Cr(VI) onto LGPH

Parameter	Value		Parameter	Value
Pseudo-first-order model			Pseudo-second-order model	
Q_e (mg/g)	315.19		Q_e (mg/g)	617.28
k_1 (L/mg)	5.44×10^{-3}		k_2	4.044×10^{-5}
R^2	0.9274		R^2	0.9978
Langmuir isotherm model			Freundlich isotherm model	
Q_m (mg/g)	621.12		K_F (mg/g)	311.94
K_L (L/mg)	4.298×10^{-2}		*1/n*	0.1048
R^2	0.9937		R^2	0.9264

CONCLUSIONS

1. A lignosulfonate-graphene porous hydrogel (LGPH) composite with excellent Cr(VI) adsorption capability was successfully prepared through a green and facile method.
2. The modification of graphene composite with lignosulfonate (LS) improved its adsorption sites, resulting in excellent Cr(VI) removal efficiency from aqueous solution.
3. The adsorption capacity of the composite for Cr(VI) was 601.2 mg/g.

ACKNOWLEDGMENTS

The authors are grateful for the financial support of the National Key Research and Development Program of China (Grant No. 2017YFB0307900), the National Natural

Science Foundation of China (Grant No. 31670590; 31670595; 31870566), the Taishan Scholars Program, and the Foundation (No.KF201820) of Key Laboratory of Pulp and Paper Science and Technology of Ministry of Education/Shandong Province of China.

REFERENCES CITED

Akram, M., Bhatti, H. N., Iqbal, M., Noreen, S., and Sadaf, S. (2017). "Biocomposite efficiency for Cr (VI) adsorption: Kinetic, equilibrium and thermodynamics studies," *Journal of Environmental Chemical Engineering* 5(1), 400-411. DOI: 10.1016/j.jece.2016.12.002

Chang, H., Wang, G., Yang, A., Tao, X., Liu, X., Shen, Y., Zheng, Z. (2010). "A transparent, flexible, low-temperature, and solution-processible graphene composite electrode," *Advanced Functional Materials* 20(17), 2893-2902. DOI: 10.1002/adfm.201000900

Chang, J. H., Kim, J., and Lee, H. (2017). "PNIPAm grafted amino-functionalized mesoporous silica for thermo-responsive chromium elimination," *Applied Surface Science* 424, 115-121. DOI: 10.1016/j.apsusc.2017.01.168

Chitpong, N., and Husson, S. M. (2017). "Polyacid functionalized cellulose nanofiber membranes for removal of heavy metals from impaired waters," *Journal of Membrane Science* 523, 418-429. DOI: 10.1016/j.memsci.2016.10.020

Gallios, G. P., and Vaclavikova, M. (2007). "Removal of chromium (VI) from water streams: A thermodynamic study," *Environmental Chemistry Letters* 6(4), 235-240. DOI: 10.1007/s10311-007-0128-8

Gao, G., Nie, L., Yang, S., Jin, P., Chen, R., Ding, D., Wang, X., Wang, W., Wu, K., Zhang, Q. (2018). "Well-defined strategy for development of adsorbent using metal organic frameworks (MOF) template for high performance removal of hexavalent chromium," *Applied Surface Science* 457, 1208-1217. DOI: 10.1016/j.apsusc.2018.06.278

Gupta, G., Birbilis, N., Cook, A., and Khanna, A. (2013). "Polyaniline-lignosulfonate/epoxy coating for corrosion protection of AA2024-T3," *Corrosion Science* 67, 256-267. DOI: 10.1016/j.corsci.2012.10.022

He, Z. W., Lü, Q. F., and Lin, Q. (2013). "Fabrication, characterization and application of nitrogen-containing carbon nanospheres obtained by pyrolysis of lignosulfonate/poly (2-ethylaniline)," *Bioresource Technology* 127, 66-71. DOI: 10.1016/j.biortech.2012.09.132

Huang, W., Liu, N., Zhang, X., Wu, M., and Tang, L. (2017). "Metal organic framework g-C_3N_4/MIL-53 (Fe) heterojunctions with enhanced photocatalytic activity for Cr(VI) reduction under visible light," *Applied Surface Science* 425, 107-116. DOI: 10.1016/j.apsusc.2017.07.050

Hummers, S. W., and Offeman, R. E. (2002). "Preparation of graphitic oxide," *Journal of the American Chemical Society* 80(6), 1339-1339.

Karnitz, O., Gurgel, L. V. A., De Melo, J. C. P., Botaro, V. R., Melo, T. M. S., de Freitas Gil, R. P., Gil, L. F. (2007). "Adsorption of heavy metal ion from aqueous single metal solution by chemically modified sugarcane bagasse," *Bioresource Technology* 98(6), 1291-1297. DOI: 10.1016/j.biortech.2006.05.013

Li, F., Wang, X., Yuan, T., and Sun, R. (2016). "A lignosulfonate-modified graphene hydrogel with ultrahigh adsorption capacity for Pb (ii) removal," *Journal of Materials*

Chemistry A 4(30), 11888-11896. DOI: 10.1039/C6TA03779H

Li, Y.H., Di, Z., Ding, J., Wu, D., Luan, Z., and Zhu, Y. (2005). "Adsorption thermodynamic, kinetic and desorption studies of Pb^{2+} on carbon nanotubes," *Water Research* 39(4), 605-609. DOI: 10.1016/j.watres.2004.11.004

Li, Z., Xiao, D., Ge, Y., and Koehler, S. (2015). "Surface-functionalized porous lignin for fast and efficient lead removal from aqueous solution," *ACS Applied Materials and Interfaces* 7(27), 15000-15009. DOI: 10.1021/acsami.5b03994

Liang, P., Liu, Y., Guo, L., Zeng, J., and Lu, H. (2004). "Multiwalled carbon nanotubes as solid-phase extraction adsorbent for the preconcentration of trace metal ions and their determination by inductively coupled plasma atomic emission spectrometry," *Journal of Analytical Atomic Spectrometry* 19(11), 1489-1492. DOI: 10.1039/B409619C

Liang, Y., Wang, X., An, W., Li, Y., Hu, J., and Cui, W. (2019). "A g-C_3N_4@ppy-rGO 3D structure hydrogel for efficient photocatalysis," *Applied Surface Science* 466, 666-672. DOI: 10.1016/j.apsusc.2018.10.059

Marcano, D. C., Kosynkin, D. V., Berlin, J. M., Sinitskii, A., Sun, Z., Slesarev, A. S., Alemany, L. B., Lu. W., and Tour, J. M. (2010). "Improved synthesis of graphene oxide," *ACS Nano* 4(8), 4806-4814. DOI: 10.1021/nn1006368

Mianehrow, H., Moghadam, M. H. M., Sharif, F., and Mazinani, S. (2015). "Graphene-oxide stabilization in electrolyte solutions using hydroxyethyl cellulose for drug delivery application," *International Journal of Pharmaceutics* 484(1), 276-282. DOI: 10.1016/j.ijpharm.2015.02.069

Murugan, A. V., Muraliganth, T., and Manthiram, A. (2009). "Rapid, facile microwave-solvothermal synthesis of graphene nanosheets and their polyaniline nanocomposites for energy storage," *Chemistry of Materials* 21(21), 5004-5006. DOI: 10.1021/cm902413c

Myglovets, M., Poddubnaya, O., Sevastyanova, O., Lindström, M. E., Gawdzik, B., Sobiesiak, M., Tsyba, M. M., Sapsay, V. I., Klymchuk, D. O., and Puziy, A. M. (2014). "Preparation of carbon adsorbents from lignosulfonate by phosphoric acid activation for the adsorption of metal ions," *Carbon* 80, 771-783. DOI: 10.1016/j.carbon.2014.09.032

Park, C. M., Wang, D., Han, J., Heo, J., and Su, C. (2019). "Evaluation of the colloidal stability and adsorption performance of reduced graphene oxide-elemental silver/magnetite nanohybrids for selected toxic heavy metals in aqueous solutions," *Applied Surface Science* 471, 8-17. DOI: 10.1016/j.apsusc.2018.11.240

Sun, J., Li, M., Zhang, Z., and Guo, J. (2019). "Unravelling the adsorption disparity mechanism of heavy-metal ions on the biomass-derived hierarchically porous carbon," *Applied Surface Science* 471, 615-620. DOI: 10.1016/j.apsusc.2018.12.050

Vu, H. C., Dwivedi, A. D., Le, T. T., Seo, S. H., Kim, E. J., and Chang, Y. S. (2017). "Magnetite graphene oxide encapsulated in alginate beads for enhanced adsorption of Cr (VI) and As (V) from aqueous solutions: Role of crosslinking metal cations in pH control," *Chemical Engineering Journal* 307, 220-229. DOI: 10.1016/j.cej.2016.08.058

Wang, Y., Xiong, Y., Wang, J., and Zhang, X. (2017). "Ultrasonic-assisted fabrication of montmorillonite-lignin hybrid hydrogel: Highly efficient swelling behaviors and super-sorbent for dye removal from wastewater," *Colloids and Surfaces A: Physicochemical and Engineering Aspects* 520, 903-913. DOI: org/10.1016/j.colsurfa.2017.02.050

Wang, Y., Du, B., Wang, J., Wang, Y., Gu, H., and Zhang, X. (2018). "Synthesis and characterization of a high capacity ionic modified hydrogel adsorbent and its application in the removal of Cr (VI) from aqueous solution," *Journal of Environmental Chemical Engineering* 6(6), 6881-6890. DOI: 10.1016/j.jece.2018.10.048

Wang, Y., Wang, Y., Yu, L., Wang, J., Du, B., and Zhang, X. (2019). "Enhanced catalytic activity of templated-double perovskite with 3D network structure for salicylic acid degradation under microwave irradiation: Insight into the catalytic mechanism," *Chemical Engineering Journal* 368, 115-128. DOI: 10.1016/j.cej.2019.02.174

Xu, T., Xue, J., Zhang, X., He, G., and Chen, H. (2017). "Ultrafine cobalt nanoparticles supported on reduced graphene oxide: Efficient catalyst for fast reduction of hexavalent chromium at room temperature," *Applied Surface Science* 402, 294-300. DOI: 10.1016/j.apsusc.2017.01.114

Xu, Y., Sheng, K., Li, C., and Shi, G. (2010). "Self-assembled graphene hydrogel *via* a one-step hydrothermal process," *ACS Nano* 4(7), 4324-4330. DOI: 10.1021/nn101187z

Yang, S. T., Chang, Y., Wang, H., Liu, G., Chen, S., Wang, Y., Liu, Y., and Cao, A. (2010). "Folding/aggregation of graphene oxide and its application in Cu^{2+} removal," *Journal of Colloid and Interface Science* 351(1), 122-127. DOI: 10.1016/j.jcis.2010.07.042

Yang, J., Wu, J., Lu, Q., and Lin, T. (2014). "Facile preparation of lignosulfonate-graphene oxide-polyaniline ternary nanocomposite as an effective adsorbent for Pb(II) ions," *ACS Sustainable Chemistry and Engineering* 2(5), 1203-1211. DOI: 10.1021/sc500030v

Yang, Y., Ding, Q., Wen, D., Yang, M., Wang, Y., Liu, N., and Zhang, X. (2018a). "Bromate removal from aqueous solution with novel flower-like Mg-Al-layered double hydroxides," *Environmental Science and Pollution Research* 25(27), 27503-27513. DOI: 10.1007/s11356-018-2781-9

Yang, Y., Dong, H., Wang, Y., He, C., Wang, Y., and Zhang, X. (2018b). "Synthesis of octahedral like Cu-BTC derivatives derived from MOF calcined under different atmosphere for application in CO oxidation," *Journal of Solid State Chemistry* 258, 582-587. DOI: 10.1016/j.jssc.2017.11.033

Yao, Z., Braidy, N., Botton, G. A., and Adronov, A. (2003). "Polymerization from the surface of single-walled carbon nanotubes-preparation and characterization of nanocomposites," *Journal of the American Chemical Society* 125(51), 16015-16024. DOI: 10.1021/ja037564y

Yao, W., Wang, J., Wang, P., Wang, X., Yu, S., Zou, Y., Hou, J., Hayat, T., Alsaedi, A., and Wang, X. (2017). "Synergistic coagulation of GO and secondary adsorption of heavy metal ions on Ca/Al layered double hydroxides," *Environmental Pollution* 229, 827-836. DOI: 10.1016/j.jcis.2010.07.042

Yi, J. Z., and Zhang, L. M. (2008). "Removal of methylene blue dye from aqueous solution by adsorption onto sodium humate/polyacrylamide/clay hybrid hydrogels," *Bioresource Technology* 99(7), 2182-2186. DOI: 10.1016/j.biortech.2007.05.028

Yıldız, S., Çekim, M., and Dere, T. (2017). "Biosorption of Cu^{2+} and Ni^{2+} ions from synthetic waters," *Applied Biochemistry and Biotechnology* 1-16. DOI: 10.1007/s12010-017-2448-x

Yu, Y., Murthy, B. N., Shapter, J. G., Constantopoulos, K. T., Voelcker, N. H., and Ellis,

A. V. (2013). "Benzene carboxylic acid derivatized graphene oxide nanosheets on natural zeolites as effective adsorbents for cationic dye removal," *Journal of Hazardous Materials* 260, 330-338. DOI: 10.1016/j.jhazmat.2013.05.041

Zhang, L., and Zhang, Y. (2014). "Adsorption characteristics of hexavalent chromium on HCB/TiO_2," *Applied Surface Science* 316, 649-656. DOI: 10.1016/j.apsusc.2014.08.045

Zhang, Z., and Yang, R. (2017). "Novel nanocomposites based on hydroxyethyl cellulose and graphene oxide," *Fibers and Polymers* 18(2), 334-341. DOI: 10.1007/s12221-017-6901-9

Zhang, X., Yang, Y., Song, L., Chen, J., Yang, Y., and Wang, Y. (2019a). "Enhanced adsorption performance of gaseous toluene on defective UiO-66 metal organic framework: Equilibrium and kinetic studies," *Journal of Hazardous Materials* 365, 597-605. DOI: 10.1016/j.jhazmat.2018.11.049

Zhang, X., Lv, X., Shi, X., Yang, Y., and Yang, Y. (2019b). "Enhanced hydrophobic UiO-66 (University of Oslo 66) metal-organic framework with high capacity and selectivity for toluene capture from high humid air," *Journal of Colloid and Interface Science* 539, 152-160. DOI: 10.1016/j.jcis.2018.12.056

Zhao, H. B., Wang, W. D., Lü, Q. F., Lin, T. T., Lin, Q., and Yang, H. (2015). "Preparation and application of porous nitrogen-doped graphene obtained by co-pyrolysis of lignosulfonate and graphene oxide," *Bioresource Technology* 176, 106-111. DOI: 10.1016/j.biortech.2014.11.035

Zhou, G., Liu, C., Chu, L., Tang, Y., and Luo, S. (2016). "Rapid and efficient treatment of wastewater with high-concentration heavy metals using a new type of hydrogel-based adsorption process," *Bioresource Technology* 219, 451-457. DOI: 10.1016/j.biortech.2016.07.038

Article submitted: April 17, 2019; Peer review completed: June 3, 2019; Revised version received and accepted: June 22, 2019; Published: July 12, 2019.
DOI: 10.15376/biores.14.3.7001-7014